HAL
open science

Atomic model of a cell-wall cross-linking enzyme in complex with an intact bacterial peptidoglycan

Paul Schanda, Sébastien Triboulet, Cédric Laguri, Catherine M Bougault, Isabel Ayala, Morgane Callon, Michel Arthur, Jean-Pierre Simorre

To cite this version:

Paul Schanda, Sébastien Triboulet, Cédric Laguri, Catherine M Bougault, Isabel Ayala, et al.. Atomic model of a cell-wall cross-linking enzyme in complex with an intact bacterial peptidoglycan. Journal of the American Chemical Society, 2014, 136 (51), pp.10. 10.1021/ja5105987 . hal-01093364

HAL Id: hal-01093364

https://hal.science/hal-01093364

Submitted on 18 Dec 2014

HAL is a multi-disciplinary open access archive for the deposit and dissemination of scientific research documents, whether they are published or not. The documents may come from teaching and research institutions in France or abroad, or from public or private research centers.

L'archive ouverte pluridisciplinaire **HAL**, est destinée au dépôt et à la diffusion de documents scientifiques de niveau recherche, publiés ou non, émanant des établissements d'enseignement et de recherche français ou étrangers, des laboratoires publics ou privés.

Atomic model of a cell-wall cross-linking enzyme in complex with an intact bacterial peptidoglycan

Paul Schanda[1,2,3,*], Sébastien Triboulet[4,5], Cédric Laguri[1,2,3], Catherine M. Bougault[1,2,3], Isabel Ayala[2,1,3], Morgane Callon[1,2,3,†], Michel Arthur[4,5] and Jean-Pierre Simorre[1,2,3,*]

[1] Univ. Grenoble Alpes, IBS, F-38044 Grenoble, France; [2] CNRS, IBS, F-38044 Grenoble, France; [3] CEA, IBS, F-38044 Grenoble, France; [4] Centre de Recherche des Cordeliers, LRMA, Equipe 12, Univ. Pierre et Marie Curie-Paris 6, UMR S 1138, 75006 Paris (France); [5] Université Paris Descartes, Sorbonne, UMR S 1138, 75006 Paris (France); INSERM, U1138, 75006 Paris (France)

ABSTRACT: The maintenance of bacterial cell shape and integrity is largely attributed to peptidoglycan, a highly cross-linked biopolymer. The transpeptidases that perform this cross-linking are important targets for antibiotics. Despite this biomedical importance to date no structure of a protein in complex with an intact bacterial peptidoglycan has been resolved, primarily due to the large size and flexibility of peptidoglycan sacculi. Here we use solid-state NMR spectroscopy to derive for the first time an atomic model of an L,D-transpeptidase from *Bacillussubtilis* bound to its natural substrate, the intact *B. subtilis* peptidoglycan. Importantly, the model obtained from protein chemical shift perturbation data shows that both domains – the catalytic domain as well as the proposed peptidoglycan recognition domain – are important for the interaction and reveals a novel binding motif that involves residues outside of the classical enzymatic pocket. Experiments on mutants and truncated protein constructs independently confirm the binding site and the implication of both domains. Through measurements of dipolar-coupling derived order parameters of bond motion we show that protein binding reduces the flexibility of peptidoglycan. This first report of an atomic model of a protein-peptidoglycan complex paves the way for the design of new antibiotic drugs targeting L,D-transpeptidases. The strategy developed here can be extended to the study of a large variety of enzymes involved in peptidoglycan morphogenesis.

Introduction

For over 70 years, peptidoglycan (PG) has played a pivotal role in the development of antibacterial chemotherapy.[1] In the quest for new drugs, the biosynthetic pathway of this ubiquitous cell wall polymer has been deciphered and essential peptidoglycan-synthesizing enzymes have been identified as putative antibacterial targets. Peptidoglycan precursors are synthesized in the cytoplasm, exported and assembled in the extracytoplasmic space by Penicillin-Binding Proteins (PBPs) that are the essential targets of β-lactam and glycopeptide antibiotics.[2] In ampicillin–resistant mutants of *Enterococcus faecium*[3] and in wild-type *Mycobacterium tuberculosis*[4] peptidoglycan cross-linking is not catalyzed by PBPs but by L,D-transpeptidases (Ldts). The Ldt from *Bacillus subtilis* (Ldt_{Bs}) was shown to catalyze this reaction *in vitro*.[5] Ldt_{Bs} consists of an N-terminal Lysin-Motif domain (LysM, residues 1 to 54) linked to the C-terminal catalytic domain (residues 55 to 169). The two domains have close contacts, remaining in a fixed relative orientation, as shown by NMR and X-ray studies.[6,7] The catalytic domains of Ldt_{Bs} and Ldts from *E. faecium* (Ldt_{fm})[8] and *M. tuberculosis* (Ldt_{Mt2}, Ldt_{Mt1})9,[10,11] display similar folds but the proteins have different domain compositions. The active site of Ldts contains a catalytic cysteine, which forms a covalent adduct with the tetrapeptide stem used as the acyl donor in the cross-linking reaction. Then, the Cys-bound tripeptide stem reacts with an adjacent peptide stem acting as an acyl acceptor, resulting in cross-linking and release of Ldt. The active-site Cys residue is also acylated by β-lactams of the carbapenem class resulting in irreversible enzyme inactivation.[3]

LysM domains are widely spread in both prokaryotes and eukaryotes[12] and are known to bind non-covalently to peptidoglycan and chitin by interacting with *N*-acetylglucosamine residues.[13] In bacteria, various enzymes involved in peptidoglycan morphogenesis during growth and cell division are known to use one or several modu-

lar LysM domains to bind to peptidoglycan.[14,15] However, little is known on the role of LysM in determining the localization of the proteins in physiologically relevant sites within the peptidoglycan layer and how recognition of specific peptidoglycan patterns by LysM domains might modulate protein function. Addressing these questions ideally requires the study of intact peptidoglycan.

Atomic-resolution studies of proteins interacting with an intact bacterial cell wall are challenging. The peptidoglycan sacculus is a gigadalton-large, dynamic and microscopically heterogeneous structure, which hampers structural investigations by X-ray crystallography as well as solution-state NMR. Electron cryotomography and atomic-force microscopy offer insight into the overall structure and architecture of peptidoglycan,[16–18] but the resolution presently obtained with these techniques does not allow resolving structural details of protein/peptidoglycan complexes at atomic resolution. The considerable flexibility of peptidoglycan[19] represents a further challenge for EM and AFM. For all the above reasons, there are currently no atomic-resolution data available with respect to the structure of proteins in interaction with intact cell wall peptidoglycan, or giving insight into the dynamics of such complexes. Fragments of peptidoglycan may be used to reconstitute complexes, which may crystallize or be amenable to solution-state NMR.[20] However, these fragments may only partially reproduce the structure and affinities of the intact cell wall and are thus insufficient in a larger picture.

Solid-state NMR (ssNMR) can circumvent these limitations, because it provides atomic resolution, independently from the size or crystallinity of the molecular system studied. SsNMR has been applied in a few cases to entire organelles, membranes or whole cells.[21,22] In the case of peptidoglycan, the repetition of of disaccharide-peptide building blocks in the polymer (see Figure 1A) and its intrinsic flexibility lead to relatively simple and well-resolved spectra. In the context of bacterial cell wall, ssNMR has proven to be a useful tool to obtain information about chemical modifications, local structure and dynamics of peptidoglycan, as well as interactions of the polymer with antibiotics and ions.[19,23,24] Low-resolution models of the architecture of peptidoglycan architecture have been proposed, for peptidoglycan from *Staphylococcus aureus* and *Enterococcus faecium* based on NMR data,[25,26] but not for peptidoglycan from *B. subtilis*. Here we show for the first time that it also provides information on the structure and dynamics of protein/PG complexes, through the investigation of the interaction of the L,D-transpeptidase Ldt_{Bs} with its physiological substrate, the peptidoglycan from *B. subtilis*.

Experimental Section

Sample preparation

Samples of *B. subtilis* peptidoglycan were prepared as described previously,[24] and outlined in the Supporting Information. Briefly, *B. subtilis* strain 168 cells were grown in rich medium, and harvested at an OD_{600} of ~0.7. The cell membranes and cytoplasm were removed by treatment with SDS, DNAse and RNAse. The samples were kept in aqueous suspension during the entire treatment, including the subsequent NMR measurements, and are thus well hydrated, retaining a high degree of flexibility.[19] Proteins were produced by bacterial over-expression using standard protocols (see Supporting Information). After extensively washing the peptidoglycan with the protein buffer (50 mM HEPES, pH 7.2) by repeated resuspension and centrifugation cycles, protein-peptidoglycan samples were obtained by incubating peptidoglycan suspensions with Ldt_{Bs} solutions (0.3-1 mM protein concentration). For solid-state NMR, this highly hydrated suspension was pelleted into either 1.3 mm, 1.6 mm or 3.2 mm ssNMR MAS rotors using a centrifugal device. A full 3.2 mm rotor, with a total sample mass of 25 mg wet protein/peptidoglycan pellet, typically contained about 3 mg of protein. Different samples were used in this study, with proteins either unlabeled, U-[$^{13}C^{15}N$]- or U-[$^{2}H^{13}C^{15}N$]-labeled. Peptidoglycan was either unlabeled (for protein-detected experiments) or U-$^{13}C^{15}N$-labeled.

NMR spectroscopy and structure calculation

All NMR experiments reported in the main text were carried out on an Agilent 600 MHz VNMRS spectrometer, operating either with a MAS solid-state equipment (1.6 mm probe for ^{1}H-detected experiments or 3.2 mm triple-resonance HXY probe for ^{13}C-detected experiments), or a room-temperature solution-state probe. Additional ^{13}C-detected experiments reported in the Supporting Information were recorded on a 1000 MHz Bruker spectrometer with a 3.2 mm HCN probe. All experiments were performed at a sample temperature of 298 K, and temperature calibration in solids was performed using external temperature calibration with KBr,[25] which was found to be in very good agreement with temperature measurement of the bulk water line relative to the DSS signal in wet protein samples. Solid-state NMR experiments used MAS frequencies of either 7.716 kHz (for the $R18_1^7$ experiment on peptidoglycan), 12 or 12.5 kHz (for ^{13}C-detected experiments on Ldt_{Bs}) or 39 kHz (for ^{1}H-detected experiments on Ldt_{Bs}), or 54 kHz (for H-N REDOR experiments shown in the Supporting Information). Details on experiments and data collection are reported in the Supporting Information. Spectra were processed with nmrPipe[26] and analyzed with CcpNmr[27] or in-house written python scripts based on NMRglue.[30] Dipolar-coupling data were fitted with the use of numeri-

cal spin simulations implemented in SIMPSON[31] (for $R18_1^7$) or GAMMA[32] (for REDOR) and in-house written python programs. Dipolar order parameters are given relative to rigid-limit values of the dipolar coupling, D_{rigid}, based on 1.12 Å and 1.02 Å bond lengths for ^{1}H-^{13}C and ^{1}H-^{15}N, respectively, i.e. $S = D_{measured}/D_{rigid}$.

Residue-specific resonance assignmenf of Ldt_{Bs} in solution (without peptidoglycan) was performed by triple-resonance experiments, as reported before.[6] The 3D hCANH spectrum of Ldt_{Bs} bound to PG was obtained using a proton-detected experiment based on cross-polarization steps,[33] as outlined in the Supporting Information.

The docking of the protein on the peptidoglycan was performed using HADDOCK[34] /CNS[35] protocols. As starting structures of the two binding partners we used the solution-NMR structure of Ldt_{Bs} and a set of ten structures of a hexameric muropeptide fragment, as described in the Supporting Information. The docking protocol used ambiguous restraints to the protein residues that showed significant chemical-shift perturbation in H-N-CA experiments (larger than twice the standard deviation over the whole sequence). For the muropeptide, where no unambiguously identified binding sites are available, all atoms were defined as passive ambiguous interaction restraints. The knowledge about the catalytic site in Ldt_{Bs}, residue C142, was exploited by adding a distance restraint between the sulfur of C142 and the carbonyl of the DAP residue in one of the peptides of the hexameric muropeptide. Best convergence was achieved when the constraint was applied to the fifth disaccharide-tetrapepeptide residue (see Figure S8). More details about the experimental and calculation procedure are described in the Supporting Information.

Results

Ldt_{Bs} tightly binds to peptidoglycan

Peptidoglycan is a highly flexible three-dimensional polymer, and its dynamic nature critically relies on the aqueous environment. Consequently, only samples containing well-hydrated pellets of peptidoglycan were used for all experiments that aim at visualizing its interactions with Ldt_{Bs} protein, and the impact of this binding on its dynamics. Upon incubating *B. subtilis* peptidoglycan suspension with purified Ldt_{Bs}, the protein concentration in the supernatant dropped (as evidenced by spectrophotometry at 280 nm), indicating that the protein binds to the peptidoglycan sacculi. Binding of Ldt_{Bs} to peptidoglycan sacculi was found to be saturable as the addition of the protein in excess to 1.5 mg per 10 mg sacculi led to recovery of excess protein in solution. In order to obtain atomistic details for this interaction, we transferred the protein/peptidoglycan sacculi suspension into MAS rotors for analysis by solid-state NMR.

In a first sample, containing unlabeled peptidoglycan and U-[^{13}C,^{15}N]-labeled Ldt_{Bs}, we visualized the state of the protein through one-dimensional ^{13}C-detected ss-NMR experiments. Three types of experiments were used that employ either (i) direct ^{13}C excitation, (ii) cross-polarization from ^{1}H to ^{13}C prior to ^{13}C-detection or (iii) scalar-coupling based refocused-INEPT transfer. The first type of experiment detects all the protein in the sample, independently of whether the protein is tightly bound to peptidoglycan or tumbling freely in the surrounding solution. In the second type of experiment, only protein bound to the (solid-like) peptidoglycan sacculi is detectable, while freely tumbling protein would be undetectable due to averaging through reorientational motion. The third type of experiment, refocused INEPT, would lead to detectable signals only in the presence of motions of large-amplitude, such as overall tumbling.[36] These experiments thus provide a qualitative picture of the protein's dynamic behavior in the presence of peptidoglycan. Intense protein signals were observed in the cross-polarization experiment indicating that Ldt_{Bs} is tightly bound to peptidoglycan, adopting the spectroscopic properties of a solid-state sample (Figure S1). In contrast, no signals were detected in a refocused-INEPT experiment (data not shown), confirming that Ldt_{Bs} is not freely tumbling. Taken together, these data reveal that upon incubation with PG, Ldt_{Bs} adopts a solid-like behavior, suggesting a strong interaction to the large, solid-like peptidoglycan sacculi with a rather long residential time (at least milliseconds or longer).

In order to obtain more quantitative insight into the dynamics of the protein in this state, we investigated the amide ^{1}H-^{15}N dipolar couplings of the protein backbone amides. The dipolar-coupling can be directly related to the order parameter that describes the motional freedom of the individual ^{1}H-^{15}N bond vector over time scales shorter than tens of microseconds. This order parameter, S, ranges from 0 for complete disorder to 1 in the absence of any local or global motion. We used a one-dimensional version of a REDOR experiment[26,27] with ^{1}H detection, and integrated the whole amide region in this measurement, to obtain an effective average value. The bulk amide H-N order parameter is S = 0.82 (Figure S2). Although this value is clearly lower than what one would expect for a completely immobilized protein in a crystal or a precipitate (where S is generally larger than 0.9[35–38]), it confirms that the protein has adopted the spectroscopic properties of a protein in the solid state (in a freely tumbling protein the dipolar-coupling order parameter is zero). The fact that the order parameter is lower than in typical crystalline samples can be understood from the fact that the protein is tightly bound to PG, which itself shows relatively large amplitude motions (see section below). Residual global flexibility of PG would necessarily impart some degree of overall motion

on the interacting Ldt_{Bs} protein. We have also measured bulk ^{15}N $R_{1\rho}$ relaxation rates in a highly deuterated protein sample at fast magic-angle spinning, as these rates are sensitive to motions on the time scales of tens of nanoseconds to microseconds. We find a bulk $R_{1\rho}$ relaxation rate of 14 ± 3 s^{-1}, significantly higher than corresponding values in microcrystalline proteins,[37–39] where typical average $R_{1\rho}$ are below 5 s^{-1}. Taken together, these dynamics measurements show that Ldt_{Bs} in the presence of peptidoglycan adopts the behavior of a protein in the solid state, but that it has a slightly higher flexibility than for proteins embedded in a crystal lattice. This peculiar protein behavior is presumably due to the flexibility of its binding partner, the peptidoglycan. These results on the protein prompted us to analyze the dynamics of peptidoglycan in the bound and unbound states.

Peptidoglycan dynamics in the protein-bound state

In order to obtain insight into the effect of protein binding on peptidoglycan conformation and dynamics, we performed ^{13}C-detected experiments on samples containing U-[^{13}C,^{15}N]-labeled peptidoglycan.

Figure 1B shows site-resolved measurements of ^{1}H-^{13}C dipolar couplings for various sites of the peptide and sugar moieties in peptidoglycan samples with and without Ldt_{Bs}. Data were acquired using an improved version[33] of a $R18_1^7$ recoupling experiment.[40] These dipolar couplings directly can be directly related to the order parameter of C-H bond motion that reflect the degree of motional freedom of the bond vectors (ranging from 0 for full flexibility to 1 for rigid sites). In the absence of protein, we find order parameters in the order of S = 0.6 for sugar ^{1}H-^{13}C bonds.^{1}H-^{13}C bonds in the peptide moieties have values in the 0.2-0.3 range. These values are clearly much lower than typical order parameters found in rigid biomolecules, such as microcrystalline, fibrillar or precipitated protein samples, that show values around 0.9 for ^{1}H-^{13}C and ^{1}H-^{15}N bonds.[37,41–43] The significant flexibility of peptidoglycan, that is reflected by these low S values, has been reported earlier for hydrated peptidoglycan.[19] In the presence of Ldt_{Bs}, the order parameters of the sugar moieties are markedly increased from S ~ 0.6 to S ~ 0.8 (Figure 1C), similar to Ldt_{Bs}'s NH order parameters discussed in the previous section. For the peptide stems of PG, which are more flexible than the sugar moieties, the presence of protein does not lead to significant changes in order parameters. ^{13}C R_1 relaxation parameters, which are sensitive to amplitudes and time scales of motion, provide a very similar picture to the one obtained from dipolar couplings (Figure 1D): the presence of protein leads to prolonged T_1 relaxation time constants of the glycan moieties, while the peptide stems have shorter T_1 relaxation times which are almost identical with and without protein. These measurements therefore unambiguously show that peptidoglycan dynamics are impacted by the presence of protein. The chemical-shift changes upon binding are much less pronounced than the changes in dynamics (Figure S3). This may be related to the known fact that sugar-protein interactions generally lead only to relatively small chemical shift perturbations.[44,45] In addition, given the steric requirements of a protein binding to peptidoglycan, we must assume that not all di-saccharide-tetrapeptide subunits are bound to protein, and our NMR signal is a sum of signals from free and bound subunits. Within the experimental sensitivity and line width of PG signals, signals from bound subunits may therefore not be distinguishable from signal of free subunits.

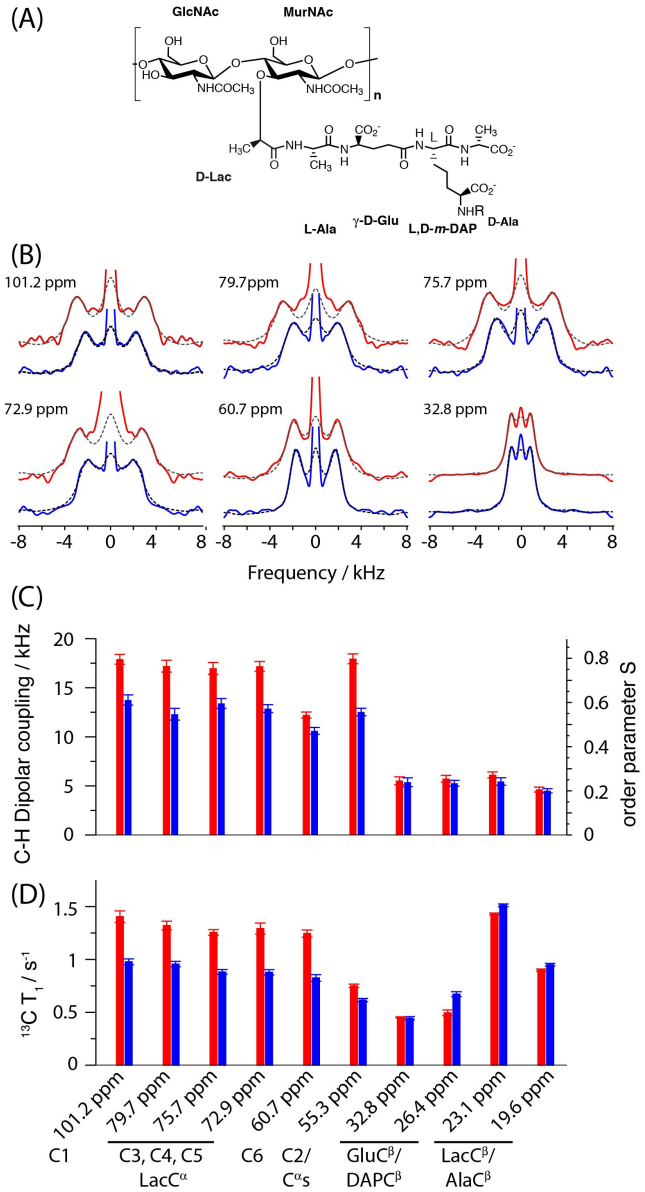

Figure 1. The impact of protein binding on peptidoglycan dynamics. (A) Chemical structure of peptidoglycan. (B) Measurement of one-bond ^{1}H-^{13}C dipolar couplings in peptidoglycan, using a windowed $R18_1^7$ sequence at a MAS fre-

quency of 7.716 kHz. Dipolar splittings are measured in the absence (blue) and presence (red) of Ldt_{Bs}. Dotted lines show best-fit curves, based on numerical simulations of the pulse sequence (see Experimental section). (C) ^{1}H-^{13}C dipolar couplings in peptidoglycan without (blue) and with (red) Ldt_{Bs}. (D) ^{13}C T_1 relaxation time constants without (blue, data similar to ref. 19) and with (red) Ldt_{Bs}.

Atomic model of the complex from ^{1}H-detected ssNMR experiments

Having demonstrated that Ldt_{Bs} binds *B. subtilis* peptidoglycan, we attempted to derive an atomic model for this complex. In order to identify the binding site on Ldt_{Bs} at atomic resolution, we investigated the chemical-shift changes upon binding by comparing the NMR spectra of the Ldt_{Bs} protein in the absence of PG (i.e. in solution) and in complex with PG (i.e. in the solid-like sample state). Care was taken to ensure that the protein, buffer and temperature conditions were identical in both cases; solution-state NMR spectra were collected with the protein sample that was subsequently incubated with PG for ssNMR. Figure 2A shows the overlay of two-dimensional proton-detected ^{1}H-^{15}N correlation spectra of U-[^{2}H,^{13}C,^{15}N] Ldt_{Bs} collected in solution without peptidoglycan (blue), and in the solid state, bound to peptidoglycan (red; collected at a MAS frequency of 39 kHz). Additional ^{13}C-detected NCA and CC spectra are shown in the Supporting Information (Figure S4). The close similarity of peak positions in the two spectra in Figure 2A immediately shows that the protein retains the same global fold upon peptidoglycan interaction. Extraction of precise site-resolved chemical values was hampered by the significant resonance overlap in the solid-state NMR spectrum of this 19 kDa protein from such 2D spectra. This prompted us to collect three-dimensional spectra. The intrinsic sensitivity of higher-dimensional spectra is lower, which is a challenge particularly in the present context, where the majority of the sample volume is occupied by peptidoglycan rather than protein. In this context, proton-detected ssNMR experiments on a deuterated protein sample turned out to be crucial. The improved sensitivity of proton-detection under fast MAS allowed the collection of a 3D (H^N)CANH^N ^{1}H-$^{13}C^{\alpha}$-^{15}N correlation experiment. Figure 2B shows excerpts from this 3D experiment, overlaid with a corresponding solution-state HNCA experiment. Figure 2C shows the chemical-shift perturbation (CSP) upon binding, i.e. the combined difference o f ^{1}H-$^{13}C^{\alpha}$-^{15}N chemical shifts, as a function of the residue number, as derived from these 3D spectra. Residues with a CSP greater than two standard deviations are represented in red on the free Ldt_{Bs} structure[6] in Figure 3A. Residues with significant chemical-shift perturbation upon the peptidoglycan interaction are located both in the LysM and catalytic domains.

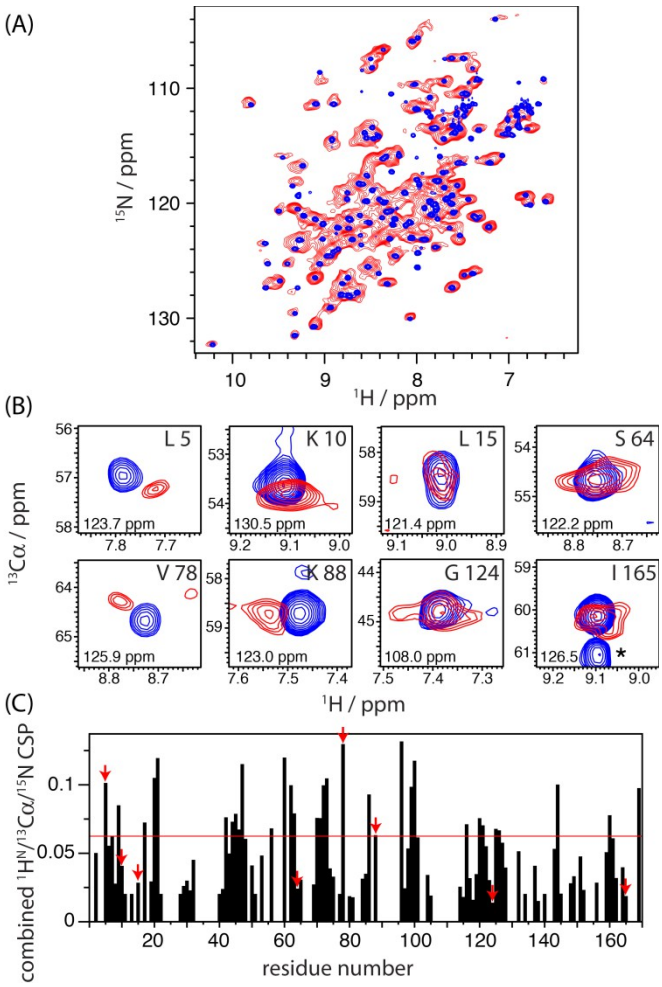

Figure 2. ssNMR characterization of the interaction between Ldt_{Bs} and *B. subtilis* peptidoglycan. A) Comparison of ^{1}H-^{15}N correlation spectra of [U-^{2}H,^{13}C,^{15}N] Ldt_{Bs} in solution (blue) and in the presence of peptidoglycan (red). The latter spectrum was collected at a MAS frequency of 39 kHz, using cross-polarization (CP) transfer steps. B) Representative excerpts from 3D ^{1}H-$^{13}C^{\alpha}$-^{15}N correlation spectra. The peak labeled with an asterisk (lower right) arises from the correlation to the C^{α} of the preceding residue 164, which cannot be observed in the solid state due to pulse sequence design. Numbers in each panel refer to the ^{15}N chemical shift at which the displayed ^{1}H-^{13}C planes were extracted. C) Combined chemical shift perturbations (CSP) between free and bound protein, calculated as the square root of the sum of the squared absolute chemical shift difference in the ^{1}H,^{13}C, ^{15}N dimensions, weighted by the relative gyromagnetic ratios. Red arrows indicate the residues shown in panel (B). The red horizontal line displays two standard deviations over all residues.

Based on these residue-specific interaction data, we calculated a structural model of the complex using HADDOCK,[34] a data-driven docking protocol based on CNS.[35] In this approach, residue-specific CSP data are

used as ambiguous distance restraints between the respective protein residues and the peptidoglycan during an energy minimization process performed on the two interacting molecules. For Ldt_{Bs}, the input structure was the solution-state NMR-derived structure of the protein.[6] For peptidoglycan, a fragment consisting of six di-saccharide-tetrapeptide subunits was chosen. This fragment is sufficiently long to cover the whole binding surface of Ldt_{Bs}. The use of longer fragments does not lead to significant changes, as it leads to (redundant) solutions, which show the same binding mode, but in which the PG fragment is translationally shifted. Peptidoglycan is a three-dimensional polymer, and Ldt_{Bs} might contact two separate PG stems. We did not consider this possibility in the docking process as the absence of structural data on PG architecture would make a three-body docking highly ambiguous and our data can be explained with a single PG fragment.

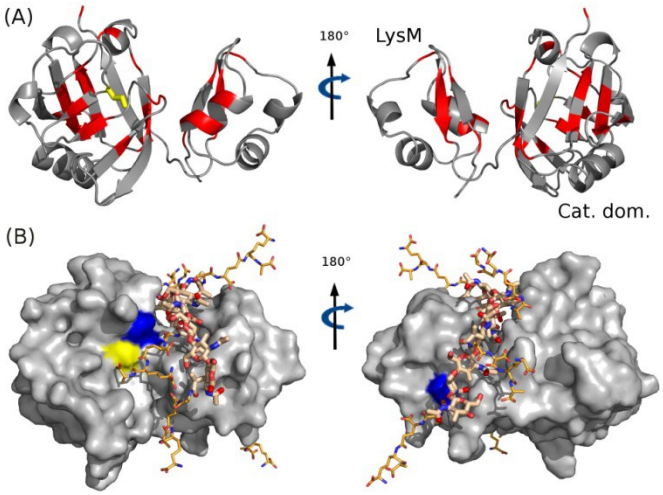

Figure 3. NMR chemical-shift perturbation (CSP) induced by the peptidoglycan on Ldt_{Bs} and result of the HADDOCK calculation. A) CSP are displayed in red on a ribbon representation of Ldt_{Bs}. The threshold shown in Figure 2C was used in this representation. B) Lowest energy structure obtained for the peptidoglycan-Ldt_{Bs} complex. The catalytic cysteine (C142) is shown in yellow. The residues shown in blue are H122 (left panel) and V47 (right panel), used for mutation experiments.

Since peptidoglycan is flexible, a set of ten structures was generated for the hexamer by an energy-minimization process, and docking was performed with all these conformers as starting structures (Figure S5). The catalytic mechanism of Ldt_{Bs} involves the formation of a covalent link between the C142 of Ldt_{Bs} and the carbonyl of DAP in the donor peptide stem.[3] For this reason, a distance restraint between the C142 sulfur and the carbonyl carbon of one of the DAP residues was used in addition to the CSP data of Figure 2C for the docking procedure. As discussed in the Supporting Information, this restraint improves the convergence of the calculation. However, the result without the restraint is similar in the sense that the final solution with the C142-restraint is among the two best-scoring solutions in a calculation performed without this restraint (Figure S7).

The lowest energy model and an ensemble of the five lowest energy structures of this calculation are presented in Figures 3B and S8, respectively. In these models, the LysM domain interacts with each of the six muropeptide subunits. Additional contacts occur between residues 90-100, 115-125, and 142 of the catalytic domain and muropeptides 2 to 5 of the hexamer. Figure S8B shows a detailed contact map, and Figure S6 illustrates the change of the PG conformation upon docking.

Mutants and isolated domains have different binding affinities than full-length wild-type Ldt_{Bs}

In order to independently validate this structural model, we explored how a perturbation of the binding site would impact the binding. To this end we performed site-directed mutagenesis of Ldt_{Bs}-residues V47 and H122 which are predicted in our structural model to be in the interaction site (shown in blue in Figure 3B). Residue V47 of the LysM domain interacts with the MurNAc and peptide moieties of the second disaccharide-peptide subunit of the hexamer, and H122 is close to the DAP residue of the fifth disaccharide-peptide. NMR spectra of the mutant proteins in solution in the absence of peptidoglycan showed that the V47C and H122A substitutions did not perturb the overall structure of Ldt_{Bs}. Moreover, the substitutions did not prevent binding of Ldt_{Bs} to peptidoglycan since pull-down experiments revealed the expected decrease in the absorbance at 280 nm in the supernatant upon incubation, similar to wild-type Ldt_{Bs}. As with wild-type protein, we performed one-dimensional ^{13}C-detected experiments to follow the behavior of the protein. The presence of the two proteins in the PG-pellet is evidenced by direct-excitation ^{13}C ssNMR spectra (Figure S1). However, the ^{1}H-^{13}C cross-polarization transfer was almost entirely suppressed in both variants, in strong contrast to the wild-type protein. This cancellation of the ^{1}H-^{13}C dipolar transfer can be explained by dynamics, such as a rapid exchange between free and bound forms of the protein, which averages out the dipolar coupling. Thus, these data show that upon mutation of V47 or H122, Ldt_{Bs} interacts less tightly with peptidoglycan and thereby changes its spectroscopic behavior. This finding confirms the implication of these residues in the complex formation.

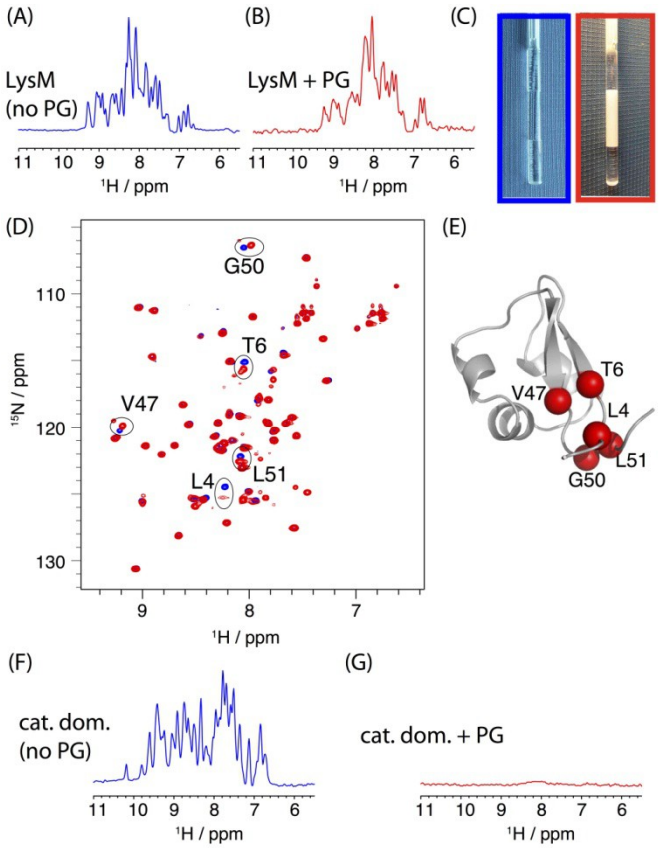

Figure 4. Solution-state NMR performed on the individual LysM and catalytic domains. (A, B) 1D ^{1}H NMR spectra of the LysM domain recorded in the absence (A, blue) or presence (B, red) of peptidoglycan. C) Photographs of the respective samples described in A) and B). (D) ^{1}H-^{15}N HSQC spectra recorded on these two LysM samples. Peaks corresponding to residues with significant chemical shift perturbation (CSP) upon peptidoglycan interaction are highlighted. Residue-wise CSP plots are shown in Figure S9. (E) Position of the backbone sites of residues with significant CSP are show as red spheres. The orientation of the LysM domain is identical to that used in Figure 3A (right panel). (F, G) 1D ^{1}H NMR spectra of the catalytic domain recorded in the absence (F, blue) or presence (G, red) of a peptidoglycan suspension. All 1D spectra resulted from 128 scans except for the spectrum in panel (G) for which 1024 scans were accumulated.

To evaluate the respective roles of the LysM and catalytic domains in the formation of the Ldt_{Bs}-peptidolgycan complex, the two domains were separately produced and individually incubated with peptidoglycan. A decrease in the supernatant absorbance upon incubation with peptidoglycan showed that both individual domains still interact with peptidoglycan. Likewise, direct-excitation ^{13}C ssNMR spectra confirmed the presence of the proteins in the peptidoglycan pellet (Figure S1). However, similar to the V47C and H122A mutants, the cross-polarization transfer was found to be very weak, showing that the interaction of the individual domains is less tight than the interaction of the full-length protein.

Interestingly, for the LysM domain, we found efficient transfer in an INEPT-type experiment under MAS. This experiment selectively detects either highly flexible parts of a protein in a solid immobilized state, or proteins tumbling freely in solution, but it generally fails to detect proteins in a rigid solid-like state. The observation of LysM in the INEPT experiment can be rationalized by a rapid exchange of LysM between a free state in solution and a peptidoglycan-bound state. This observation prompted us to perform solution-state NMR experiments on the peptidoglycan/LysM slurry without MAS. Indeed, LysM is detected in solution-state NMR in the presence of peptidoglycan (Figure 4). 2D ^{1}H-^{15}N solution-state HSQC correlation spectra of LysM in the absence and presence of peptidoglycan allowed identification of the perturbed residues upon interaction (Figure 4D). Mapping the corresponding CSP data (Panel 4E and Figure S9) identifies the β-sheet structure of LysM as the peptidoglycan interaction site. This part is also involved in the interaction within the full-length protein. This structural element also comprises V47 that was shown to be important in the interaction from the above mutation experiments.

The catalytic domain shows a slightly different behavior. Unlike LysM, the protein is not detected in INEPT experiments (Figure 4G), showing that it is not in fast exchange between bound and free states. The cross-polarization (CP) transfer is also inefficient (Figure S1), contrasting with the behavior of full-length Ldt_{Bs}, which suggests that the catalytic domain is not tightly interacting with peptidoglycan. A possible explanation for this observed behavior is an exchange between different states (different bound state(s) and possibly also free states) on a microsecond-to-millisecond time scale. Such a dynamic exchange regime would render both INEPT and CP transfers inefficient.

Taken together, all the MAS ssNMR and solution-state NMR spectra show that the individual domains of Ldt_{Bs} interact with peptidoglycan and that the LysM binding sites are similar for the isolated domain and for the full-length protein. However, the affinities of individual domains are clearly lower than the affinity of full-length Ldt_{Bs}. This apparent reliance on both domains for high-affinity interaction is in agreement with our structural model, in which both domains make extensive contacts with peptidoglycan.

It is interesting to note that the interaction site of peptidoglycan on the LysM domain of Ldt_{Bs} differs from the one observed for other LysM domains in complex with short soluble oligosaccharides.[12,46,47] A comparison of the structural model proposed here with a crystal structure of the fungal protein Ecp6 in complex with a short chitin fragment is shown in Figure S10 in the Supporting Infor-

mation. This comparison reveals that the binding site of chitin does not involve LysM's β-sheet, but is rather located at the helix adjacent to it (the helix shown on the left in Figure 4E). In the case of Ldt_{Bs} studied here, this part of LysM is not involved in the interaction. The apparent difference between the interaction modes in these two cases might arise from the different domain organization of the considered proteins, Ldt_{Bs} and Ecp6. While in Ldt_{Bs} the catalytic domain is close to LysM's β-sheet, it is on the opposite side of LysM in Ecp6 (Figure S10). As a consequence, the glycan fragments in the two cases, peptidoglycan and chitin, respectively, bind in the groove formed by LysM and the catalytic domain. The orientation of peptidoglycan we find here enables the peptide branch to contact the catalytic Cys-142 residue, while the binding mode observed in the Ecp6 complex would place the peptidoglycan fragment further away from Ldt_{Bs}'s catalytic site. Interestingly, the highly conserved LysM residues (residues G12, D13, T14 and G43 in Ldt_{Bs}) are located in between these two binding sites, such that they can be expected to be involved in complexes formed on either of the two interaction sites. Our data might thus point to some plasticity of interaction modes in LysM domains, that seems to depend on the structural context of LysM in the full-length protein.

Discussion

Peptidoglycan cross-linking by Ldt_{Bs} and related L,D-transpeptidases involves two stem peptides that act as acyl donor and acyl acceptor. In the first step of the transpeptidation reaction, the catalytic cysteine forms a covalent thioester with the backbone carbonyl of the third residue of the acyl donor stem. This reaction can be blocked by β-lactam antibiotics of the carbapenem class, which also acylate the catalytic cysteine. The NMR structure of Ldt_{fm} L,D-transpeptidase covalently bound to the ertapenem carbapenem has recently been reported.[48] Figure 5A shows the superposition of this acylenzyme structure with the model derived here for the peptidoglycan-Ldt_{Bs} complex. Interestingly, the peptide stem of the fifth disaccharide-peptide subunit occupies the antibiotic pocket in our HADDOCK model. Thus, this peptide stem is likely to occupy the position of the acyl donor of the transpeptidation reaction.

To explore possible locations of the acceptor stem, we have represented our model in the context of a complete peptidoglycan structural model generated from a regular network (Figure 5B). To generate this new model, the glycosidic chain of the complete peptidoglycan structure was superimposed with the muropeptides hexamer of the HADDOCK model. As a result, one of the muropeptides interacts through its disaccharide motif and peptide stem with the LysM and catalytic domains. In this muropeptide, the backbone carbonyl of the diaminopimelic acid in the third position of the stem peptide points towards the catalytic cysteine, playing the role of the acyl donor. At the same time, the peptide stem attached to a remote glycosidic chain points towards the catalytic cysteine, mimicking the acyl acceptor. This tentative model proposes the possible localization of the different partners required for the transpeptidation reaction.

It is interesting to revisit the dynamics data shown in Figure 1 in the light of the proposed model. The binding of Ldt_{Bs} to peptidoglycan leads to rigidifaction of the glycan part, but much less of the peptide part of peptidoglycan. In the structural model proposed here, the glycan parts form tight interactions in the groove formed by the LysM and catalytic domains of Ldt_{Bs} (Figure S8B), whereas the peptide parts are contacting surface residues outside the groove. It thus appears reasonable that the rigidification of the glycan strands is more pronounced than the rigidification of the peptides. It is likely that another mechanism contributes to the rigidification of peptidoglycan upon protein binding: our dynamics data do not point to two different sets of dynamic regimes for protein-bound and free di-saccharide-tetrapeptide subunits, respectively, but rather suggest a general stiffening of subunits directly bound to Ldt_{Bs} well as non-bound subunits. (Dipolar splittings in Figure 1B are well fitted with a single order parameter.) A reason for such a general rigidification might be found in the increased mass and hydrodynamic radius of the network of protein-loaded peptidoglycan subunits, as compared to peptidoglycan without bound protein. Through the increased hydrodynamic radius and inertia, protein binding would lead to a general reduction of mobility, akin to the reduced motion of beads on a string as compared to the string without beads.

Conclusions

In summary, we determined here the first atomic-resolution model of a protein (the L,D-transpeptidase Ldt_{Bs}) bound to intact peptidoglycan sacculi, based on solid-state NMR data. The binding mode of peptidoglycan in this model involves both the LysM and catalytic domains of Ldt_{Bs}. The glycosidic chain is located in the groove between the two domains and in this orientation one of the peptide stems can reach the catalytic cysteine residue. The inferred importance of both domains for high-affinity is supported by NMR experiments performed with isolated domains as well as site-directed mutagenesis. Our dipolar-coupling data show that peptidoglycan still retains considerable flexibility when protein is bound, although less than in the unbound state.

Proton-detected ssNMR has been found to be crucial in order to obtain the structural information reported here, and this study thus provides another example of the versatility of ^{1}H-detection in ssNMR.[33,49,50] The

methodology employed here offers a general strategy for the structural investigation of protein/cell-wall complexes. It may significantly contribute in designing future antibiotics, which do not only target the catalytic site, but also the complete binding interface on the protein.

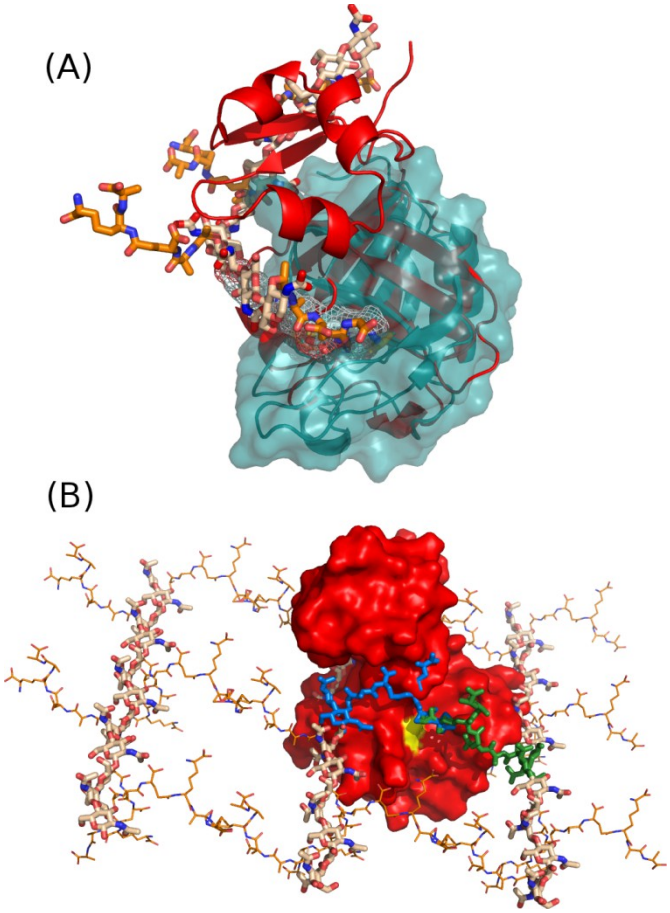

Figure 5. Possible localization of the peptidoglycan peptide stems into the catalytic pocket. A) Superimposition of our HADDOCK Ldt_{Bs}:peptidoglycan-hexamer model (Ldt_{Bs} cartoon structure in red and peptidoglycan in orange sticks) with the Ldt_{fm} acylenzyme structure (cyan cartoon and surface), with ertapenem (grey mesh). A peptide stem of peptidoglycan is localized in the same acyl donor pocket as the carbapenem antibiotic. B) Extension of our HADDOCK Ldt_{Bs}:peptidoglycan-hexamer model to a complete peptidoglycan polymer. The hexamer muropeptides of our model was overlapped with one of the glycosidic chain of the complete peptidoglycan polymer. The peptidoglycan was modeled using a threefold axis for the glycan chains. The peptide conformation was adapted to allow the cross-linking between adjacent glycan chains.[24] Possible acceptor and donor peptide stems are represented in green and blue, respectively. The catalytic cysteine is shown in yellow.

ASSOCIATED CONTENT

Supporting Information. The structural models reported here have been deposited in the PDB (accession code 2mtz), and the chemical-shift data have been deposited in the BioMagResBank (accession code 25192). Details about sample preparation, about all NMR experiments and HADDOCK docking protocols; more HADDOCK calculations with different restraints; comparison of LysM-oligosaccharide interaction sites in two different protein complexes; CSP data of free and peptidoglycan-interacting LysM domain. This material is available free of charge via the Internet at http://pubs.acs.org.

AUTHOR INFORMATION

Corresponding Authors

* paul.schanda@ibs.fr; jean-pierre.simorre@ibs.fr

Present Addresses

†Biozentrum Basel, Klingelbergstrasse 50 / 70
CH - 4056 Basel, Switzerland

ACKNOWLEDGMENT

This work was financially supported by the French Research Agency ANR (ANR 10-PDOC-011-01, ANR ANR-11-BSV5-0024). This work used the platforms of the Grenoble Instruct centre (ISBG; UMS 3518 CNRS-CEA-UJF-EMBL) with support from FRISBI (ANR-10-INSB-05-02) and GRAL (ANR-10-LABX-49-01) within the Grenoble Partnership for Structural Biology (PSB). Access to high-field NMR machines at CRMN Lyon trough IR-RMN THC (FR 3050 CNRS) and CERM Florence through Bio-NMR (FP7, Project Number 261863, Bio-NMR) is acknowledged. P.S. acknowledges support from the European Research Council (ERC-Stg-2012-311318-ProtDyn2Function). S.T. was supported by the Project Open Collaborative Model for Tuberculosis Lead Optimization (ORCHID, 261378) under the European 7th Framework Program. We thank Drs. Sabine Hediger and Gaël DePaëpe for discussions and for access to a spectrometer, and Dr. Axel Gansmüller for help with the dipolar coupling measurement.

REFERENCES

(1) Silver, L. L. *Ann. N. Y. Acad. Sci.* **2013**, *1277*, 29.

(2) Matteï, P. J.; Neves, D.; Dessen, A. *Curr. Opin. Struct. Biol.* **2010**.

(3) Mainardi, J.-L.; Hugonnet, J.-E.; Rusconi, F.; Fourgeaud, M.; Dubost, L.; Moumi, A. N.; Delfosse, V.; Mayer, C.; Gutmann, L.; Rice, L. B.; Arthur, M. *J. Biol. Chem.* **2007**, *282*, 30414.

(4) Lavollay, M.; Arthur, M.; Fourgeaud, M.; Dubost, L.; Marie, A.; Veziris, N.; Blanot, D.; Gutmann, L.; Mainardi, J.-L. *J. Bacteriol.* **2008**, *190*, 4360.

(5) Magnet, S.; Arbeloa, A.; Mainardi, J.-L.; Hugonnet, J.-E.; Fourgeaud, M.; Dubost, L.; Marie, A.; Delfosse, V.; Mayer, C.; Rice, L. B.; Arthur, M. *J. Biol. Chem.* **2007**, *282*, 13151.

(6) Lecoq, L.; Bougault, C.; Hugonnet, J.-E.; Veckerlé, C.; Pessey, O.; Arthur, M.; Simorre, J.-P. *Structure.* **2012**, *20*, 850.

(7) Bielnicki, J.; Devedjiev, Y.; Derewenda, U.; Dauter, Z.; Joachimiak, A.; Derewenda, Z. S. *Proteins.* **2006**, *62*, 144.

(8) Biarrotte-Sorin, S.; Hugonnet, J.-E.; Delfosse, V.; Mainardi, J.-L.; Gutmann, L.; Arthur, M.; Mayer, C. *J. Mol. Biol.* **2006**, *359*, 533.

(9) Kim, H. S.; Kim, J.; Im, H. N.; Yoon, J. Y.; An, D. R.; Yoon, H. J.; Kim, J. Y.; Min, H. K.; Kim, S.-J.; Lee, J. Y.; Han, B. W.; Suh, S. W. *Acta Crystallogr. Sect. D-Biological Crystallogr.* **2013**, *69*, 420.

(10) Correale, S.; Ruggiero, A.; Capparelli, R.; Pedone, E.; Berisio, R. *Acta Crystallogr. Sect. D-Biological Crystallogr.* **2013**, *69*, 1697.

(11) Böth, D.; Steiner, E. M.; Stadler, D.; Lindqvist, Y.; Schnell, R.; Schneider, G. *Acta Crystallogr. Sect. D-Biological Crystallogr.* **2013**, *69*, 432.

(12) Buist, G.; Steen, A.; Kok, J.; Kuipers, O. P. *Mol. Microbiol.* **2008**, *68*, 838.

(13) Garvey, K. J.; Saedi, M. S.; Ito, J. *Nucleic Acids Res.* **1986**, *14*, 10001.

(14) Bateman, A.; Bycroft, M. *J. Mol. Biol.* **2000**, *299*, 1113.

(15) Siewering, K.; Jain, S.; Friedrich, C.; Webber-Birungi, M. T.; Semchonok, D. A.; Binzen, I.; Wagner, A.; Huntley, S.; Kahnt, J.; Klingl, A.; Boekema, E. J.; Søgaard-Andersen, L.; van der Does, C. *Proc. Natl. Acad. Sci. U. S. A.* **2014**, *111*, E953.

(16) Li, Z.; Jensen, G. J. *Curr. Opin. Microbiol.*, 2009, *12*, 333–340.

(17) Dupres, V.; Alsteens, D.; Andre, G.; Dufrêne, Y. F. *Trends Microbiol.*, 2010, *18*, 397–405.

(18) Turner, R. D.; Vollmer, W.; Foster, S. J. *Mol. Microbiol.*, 2014, *91*, 862–874.

(19) Kern, T.; Giffard, M.; Hediger, S.; Amoroso, A.; Giustini, C.; Bui, N. K.; Joris, B.; Bougault, C.; Vollmer, W.; Simorre, J.-P. *J. Am. Chem. Soc.* **2010**, *132*, 10911.

(20) Lehotzky, R. E.; Partch, C. L.; Mukherjee, S.; Cash, H. L.; Goldman, W. E.; Gardner, K. H.; Hooper, L. V. *Proc. Natl. Acad. Sci. U. S. A.* **2010**, *107*, 7722.

(21) Kulminskaya, N. V; Pedersen, M. Ø.; Bjerring, M.; Underhaug, J.; Miller, M.; Frigaard, N.-U.; Nielsen, J. T.; Nielsen, N. C. *Angew. Chem. Int. Ed.* **2012**, *51*, 6891.

(22) Renault, M.; Cukkemane, A.; Baldus, M. *Angew. Chem. Int. Ed.* **2010**, *49*, 8346.

(23) Takahashi, H.; Ayala, I.; Bardet, M.; De Paëpe, G.; Simorre, J.-P.; Hediger, S. *J. Am. Chem. Soc.* **2013**, 130130133309007.

(24) Kern, T.; Hediger, S.; Müller, P.; Giustini, C.; Joris, B.; Bougault, C.; Vollmer, W.; Simorre, J.-P. *J. Am. Chem. Soc.* **2008**, *130*, 5618.

(25) Patti, G. J.; Sung, J. K.; Schaefer, J. *Biochemistry* **2008**, *47*, 8378.

(26) Sharif, S.; Singh, M.; Kim, S. J.; Schaefer, J. *J. Am. Chem. Soc.* **2009**, *131*, 7023.

(27) Thurber, K. R.; Tycko, R. *J. Magn. Reson.* **2009**, *196*, 84.

(28) Delaglio, F.; Grzesiek, S.; Vuister, G.; Zhu, G.; Pfeifer, J.; Bax, A. *J. Biomol. NMR* **1995**, *6*, 277.

(29) Vranken, W. F.; Boucher, W.; Stevens, T. J.; Fogh, R. H.; Pajon, A.; Llinas, M.; Ulrich, E. L.; Markley, J. L.; Ionides, J.; Laue, E. D. *Proteins.* **2005**, *59*, 687.

(30) Helmus, J. J.; Jaroniec, C. P. *J. Biomol. NMR* **2013**.

(31) Bak, M.; Rasmussen, J. T.; Nielsen, N. C. *J. Magn. Reson.* **2000**, *147*, 296.

(32) Smith, S.; Levante, T.; Meier, B.; Ernst, R. *J. Magn. Reson.* **1994**, *106*, 75.

(33) Barbet-Massin, E.; Pell, A. J.; Retel, J.; Andreas, L. B.; Jaudzems, K.; Franks, W. T.; Nieuwkoop, A. J.; Hiller, M.; Higman, V. A.; Guerry, P.; Bertarello, A.; Knight, M. J.; Felletti, M.; Le Marchand, T.; Kotelovica, S.; Akopjana, I.; Tars, K.; Stoppini, M.; Bellotti, V.; Bolognesi, M.; Ricagno, S.; Chou, J. J.; Griffin, R. G.; Oschkinat, H.; Lesage, A.; Emsley, L.; Herrmann, T.; Pintacuda, G. *J. Am. Chem. Soc.* **2014**, 140818104742001.

(34) Dominguez, C.; Boelens, R.; Bonvin, A. M. J. J. *J. Am. Chem. Soc.* **2003**, *125*, 1731.

(35) Brunger, A. T. *Nat. Protoc.* **2007**, *2*, 2728.

(36) Andronesi, O. C.; Becker, S.; Seidel, K.; Heise, H.; Young, H. S.; Baldus, M. *J. Am. Chem. Soc.* **2005**, *127*, 12965.

(37) Haller, J. D.; Schanda, P. *J Biomol NMR* **2013**, *57*, 263.

(38) Lewandowski, J. R.; Sass, H. J.; Grzesiek, S.; Blackledge, M.; Emsley, L. *J. Am. Chem. Soc.* **2011**, *133*, 16762.

(39) Krushelnitsky, A.; Zinkevich, T.; Reichert, D.; Chevelkov, V.; Reif, B. *J. Am. Chem. Soc.* **2010**, *132*, 11850.

(40) Zhao, X.; Eden, M.; Levitt, M. H. *Chem. Phys. Lett.* **2001**, *342*, 353.

(41) Franks, W.; Zhou, D.; Wylie, B.; Money, B.; Graesser, D.; Frericks, H.; Sahota, G.; Rienstra, C. *J. Am. Chem. Soc.* **2005**, *127*, 12291.

(42) Chevelkov, V.; Fink, U.; Reif, B. *J. Am. Chem. Soc.* **2009**, *131*, 14018.

(43) Yang, J.; Tasayco, M.; Polenova, T. *J. Am. Chem. Soc.* **2009**, *131*, 13690.

(44) Canales, A.; Angulo, J.; Ojeda, R.; Bruix, M.; Fayos, R.; Lozano, R.; Giménez-Gallego, G.; Martín-Lomas, M.; Nieto, P. M.; Jiménez-Barbero, J. *J. Am. Chem. Soc.* **2005**, *127*, 5778.

(45) Laguri, C.; Sapay, N.; Simorre, J. P.; Brutscher, B.; Imberty, A.; Gans, P.; Lortat-Jacob, H. *J. Am. Chem. Soc.* **2011**.

(46) Mesnage, S.; Dellarole, M.; Baxter, N. J.; Rouget, J.-B.; Dimitrov, J. D.; Wang, N.; Fujimoto, Y.; Hounslow, A. M.; Lacroix-Desmazes, S.; Fukase, K.; Foster, S. J.; Williamson, M. P. *Nat. Commun.* **2014**, *5*, 4269.

(47) Sánchez-Vallet, A.; Saleem-Batcha, R.; Kombrink, A.; Hansen, G.; Valkenburg, D.-J.; Thomma, B. P.; Mesters, J. R. *Elife* **2013**, *2*, e00790.

(48) Lecoq, L.; Dubée, V.; Triboulet, S.; Bougault, C.; Hugonnet, J. E.; Arthur, M.; Simorre, J. P. *ACS Chem. Biol.* **2013**, *8*, 1140.

(49) Linser, R.; Dasari, M.; Hiller, M.; Higman, V.; Fink, U.; Lopez del Amo, J.-M.; Markovic, S.; Handel, L.; Kessler, B.; Schmieder, P.; Oesterhelt, D.; Oschkinat, H.; Reif, B. *Angew Chem Int. Ed. Engl.* **2011**, *50*, 4508.

(50) Ward, M. E.; Shi, L.; Lake, E.; Krishnamurthy, S.; Hutchins, H.; Brown, L. S.; Ladizhansky, V. *J. Am. Chem. Soc.* **2011**, *133*, 17434.

TOC Figure.